Magnetic coupling induced by hole doping in perovskites $La_{1-x}Ca_xMnO_3$: A neutron scattering study

F. Moussa, M. Hennion, G. Biotteau, and J. Rodríguez-Carvajal
Laboratoire Léon Brillouin, CEA-CNRS, CE Saclay, 91191 Gif sur Yvette Cedex, France

L. Pinsard and A. Revcolevschi
Laboratoire de Chimie des Solides, Université Paris–Sud, 91405 Orsay Cedex, France
(Received 19 February 1999)

Elastic and inelastic neutron scattering has been used to study static and dynamic magnetic properties in Ca-doped $LaMnO_3$ perovskites in the region of low doping (5% and 8%) and to determine the phase diagram. In addition to the spin-wave branch related to the superexchange coupling between Mn ions (ferromagnetic in the basal planes and antiferromagnetic along the direction perpendicular to them), a new type of ferromagnetic spin excitation branch is found induced by hole doping. This is revealed by well-defined propagative spin wave modes with a gap and a nearly isotropic dispersion law at small q values: $\omega=\omega_0+Dq^2$. At T_N, these modes change from a collective to a diffusive character. The width in energy associated to the quasielastic scattering exhibits a similar dispersion law: $\Gamma=\Gamma_0+dq^2$. All these results are compared with other experimental results on similar compounds and discussed in the frame of existing theories. [S0163-1829(99)02241-9]

I. INTRODUCTION

Manganite compounds with general formula $R_{1-x}A_xMnO_3$ (R=La, Pr, Nd, etc. and A=Ca, Sr, Ba, Pb, etc.) have recently attracted a renewed interest because of their spectacular transport properties, in particular their colossal magnetoresistance (CMR) around a critical value x_c. For a doping $x \geqslant x_c$, these materials undergo a transition from a high-temperature paramagnetic insulating state to a low-temperature ferromagnetic metallic state. The physics driving this transition is not yet fully understood.

In the double-exchange model of Zener[1] the mobility of the holes is favored by a ferromagnetic spin alignment. But is the thermal spin disorder alone responsible for the high-temperature insulating phase? What is the role of the formation of magnetic and/or lattice polarons?[2,3] May any spatial inhomogeneities in electronic density[4–8] play a part at the transition?[9,10]

We address these questions by studying compounds at low doping, $x<x_c$, where structural and magnetic transitions take place although the systems remain semiconducting, in the whole temperature range. In contrast, much attention has been payed to systems with $x \geqslant x_c$ with CMR properties in the last years. Approaching the insulator-metal transition at low temperature by varying x, we hope to evidence possible precursor effects. Among possible A cations, we have chosen calcium since $La_{1-x}Ca_xMnO_3$ exhibits the most striking CMR effects.[11] This may be related to a stronger oxygen octahedron tilt induced by the smaller tolerance factor[12] than in the case of Sr, for instance. These Ca-doped compounds were studied in the pioneering experimental and theoretical works of Goodenough,[13] Wollan and Koehler,[14] de Gennes,[15] and Matsumoto.[16]

In a previous work, we have determined both the magnetic and crystalline structure of pure $LaMnO_3$.[17,18] In addition, spin-wave measurements have allowed the determination of the superexchange integrals and the single ion anisotropy constant.[17,19] In one of the first accounts of the spin dynamics concerning the $x=0.05$ compound, it was reported that a new spin-wave branch appears in addition to that attributed to superexchange.[20] Also, a diffuse scattering of magnetic origin, showing a q modulation, was observed and interpreted as coming from a liquidlike distribution of magnetic droplets.[21]

Here we report the main results concerning the phase diagram, the superexchange coupling constants, and the extra magnetic coupling induced by hole doping in Ca-doped compounds with $x=0.05$ and 0.08. This paper is organized as follows: after giving some experimental details in Sec. II, we present the phase diagram in Sec. III. In Sec. IV we report the spin-wave dispersion branches. In Sec. V we present the results concerning the temperature behavior of both excitations. Finally, in Sec. VI, our results are discussed in a larger context.

II. EXPERIMENT

Single crystals of $La_{1-x}Ca_xMnO_3$ with $x=0.05$ and 0.08 with a volume of about 0.5 cm^3 and a 0.6° mosaic spread, have been grown by the floating-zone method in an image furnace. This technique has been fully described in Ref. 17.

Each sample was mounted on an aluminum block in a double stage helium closed cryogenerator. The regulation of temperature was driven by a digital temperature controller and the stability was better than ± 0.03 K in the whole temperature range.

Neutron-scattering experiments were performed on triple-axis spectrometers installed at either thermal or cold neutron sources at the reactor ORPHEE of the Laboratoire Léon Brillouin. These spectrometers are equipped with vertically focusing monochromators. For elastic measurements, flat analyzers were used. An incident neutron beam, with a wave vector $k_i=2.662$ $Å^{-1}$ and a graphite filter was selected.

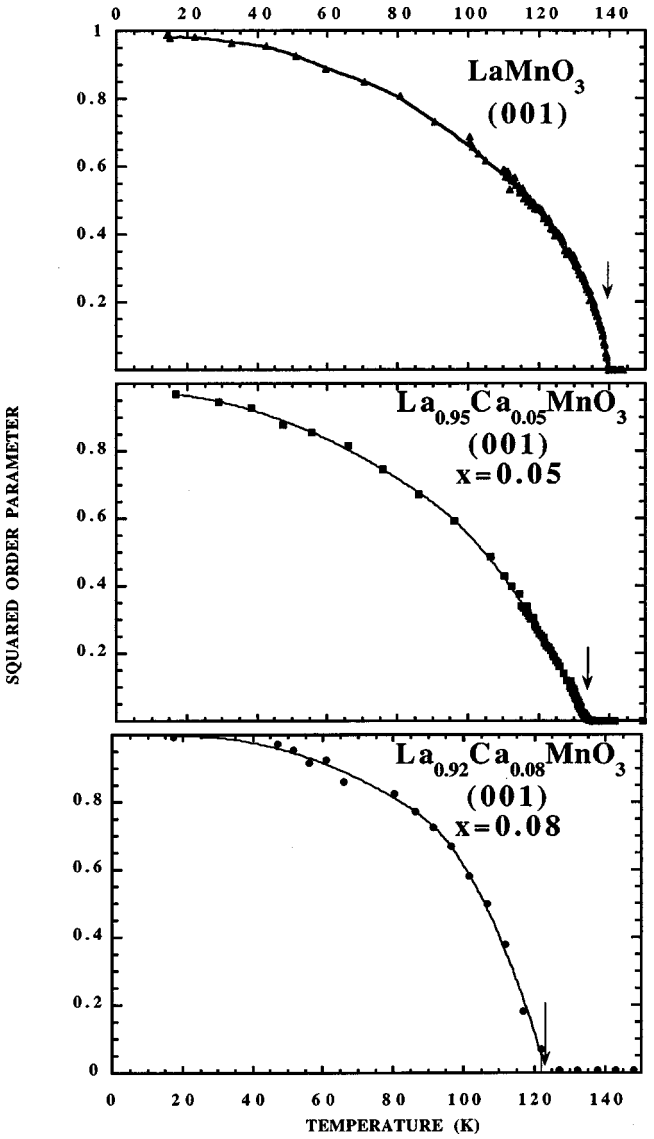

FIG. 1. Temperature dependence of the normalized intensity of the AF (001) Bragg peak for $x=0,0.05,0.08$. The arrow shows T_N.

Neutrons with $k_i=1.55$ Å^{-1}, filtered by a beryllium crystal, were chosen when a better q resolution was required. For inelastic neutron-scattering measurements, we used a horizontally focusing analyzer to increase the signal. At low temperature, positive-energy transfer scans were performed at constant scattered neutron wave vector k_f with appropriate filter in front of the analyzer. Different final wave vectors ($k_f=2.662$ Å^{-1}, $k_f=1.97$ Å^{-1}, $k_f\leqslant 1.55$ Å^{-1}) were selected according to the energy ranges of the study. All our spectra have been fitted with appropriated scattering functions $S(\mathbf{Q},\omega)$ convoluted with the resolution function of the spectrometers.

As a result of high-temperature structural phase transitions from nearly cubic phases, the three studied crystals of $Pbnm$ symmetry ($c/\sqrt{2}<a<b$) are twinned at room temperature. That means a given direction in the scattering plane corresponds to two, or even three, distinct axes of the orthorombic domains. This problem and the way it may be solved was widely explained in Ref. 17. The three studied crystals have been aligned with a horizontal scattering plane

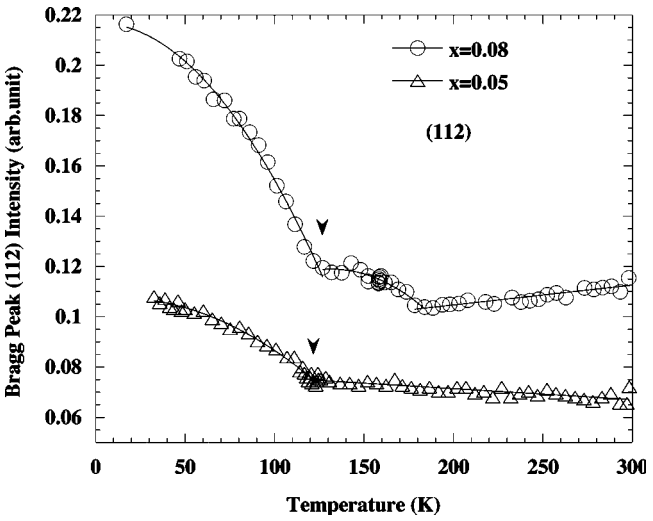

FIG. 2. Temperature dependence of the intensity of the F (112) Bragg peak for $x=0.05,0.08$. In the case of $x=0.08$, it appears a hollow at $T=175$ K may be due to a structural phase transition. This must be clarified in a future work. Lines are guides for the eye. The arrow shows T_C.

including the directions: [110] and [001], i.e., a^*+b^* and c^*. (Throughout the paper, we will use orthorhombic notations.)

III. ELASTIC-SCATTERING MEASUREMENTS

The thermal evolution of the intensity of the Bragg peak (001), $I(001)$, makes it possible the determination of the Néel temperature (Fig. 1). In order to compare the values of T_N for the three different systems, $x=0$, 0.05, and 0.08, we have plotted the square magnetic order parameter, i.e.,

$$\mu^2(T)=[I(001)_T-I(001)_{HT}]/[I(001)_{T=0\ \mathrm{K}}-I(001)_{HT}].$$

[$I(001)_{HT}$ is a spurious intensity due to a not fully filtered second order.] The evolution of $\mu^2(T)$ is displayed in Fig. 1 for the three compounds. The values of T_N are found to decrease with x. Moreover, in the case of doped compounds ($x=0.05$ and 0.08), the temperature behavior of the intensity of the Bragg peaks (002), (110), and (112) (Fig. 2), has allowed us to detect a further ferromagnetic phase transition: the intensity of (002) Bragg peak is almost constant in the whole range of temperature, whereas the intensities of (110) and (112) Bragg peaks increase on cooling, with a sudden change of the slope below a critical temperature, T_C. As an example, the thermal variation of the (112) Bragg-peak intensity of both crystals is shown in Fig. 2. We deduced from these results that a ferromagnetic component appears along the c axis. For the $x=0.05$ compound, as T_C is lower than T_N, we concluded that the system displays a canted antiferromagnetic phase (CAF) below T_C. In the case of the $x=0.08$ compound T_C is $\geqslant T_N$, so that the system becomes first slightly ferromagnetic (F) then CAF. Assuming Mn spins lying in the b-c plane, we have determined their deviation angle θ from b (Fig. 3). We recall that even in pure $LaMnO_3$, due to a small antisymmetric Dzialoshinski-Moriya coupling, F spin component has been found[16] but the canting angle is too small to be detected by neutron diffrac-

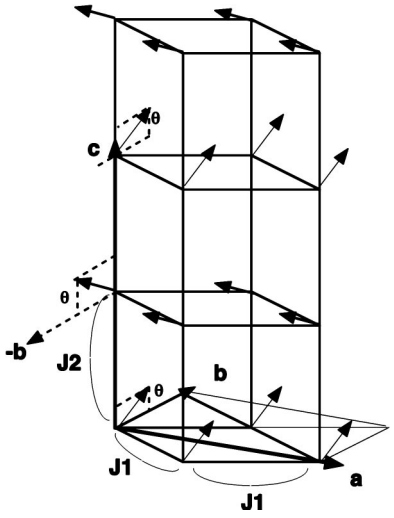

FIG. 3. Magnetic structure of $La_{1-x}Ca_xMnO_3$. Magnetic moments are assumed to be confined in (b,c) plane and are tilted by a canting angle θ with respect to b or $-b$.

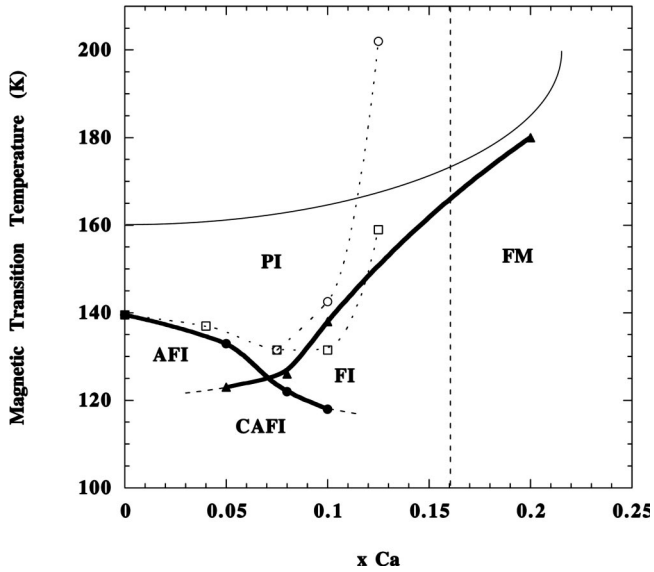

FIG. 4. Magnetic phase diagram of $La_{1-x}Ca_xMnO_3$ system. Full circle, T_N; full triangle, T_C. Points at $x=0.1$ and 0.20 have been added, they are obtained from preliminary results. The thin line represents the beginning of the magnetic phase diagram in the same system, reported by Schiffer *et al.* (Ref. 23). Empty symbols represent the phase diagram in the low doping rate range of the $La_{1-x}Sr_xMnO_3$ system reported by Kawano *et al.* (Ref. 22). Thick lines are guides for the eye.

tion. All these results are gathered in Table I. The so-built magnetic phase diagram is shown in Fig. 4. Two lines of magnetic transitions cross near $x=0.08$: T_N decreases while T_C increases with doping. The occurrence of a canted antiferromagnetic state is qualitatively in agreement with the predictions of de Gennes[15] in the frame of a mean-field model. However in our case, the slopes are much less steep than in de Gennes's calculations. Actually, the homogeneous picture of the so-called canted antiferromagnetic state, where a ferromagnetic component exists on *all Mn sites*, and the inhomogeneous picture of coexisting ferromagnetic and antiferromagnetic regions as proposed by several authors,[4–8] cannot be differentiated without a magnetic field. Several arguments are in favor of a homogeneous magnetic phase, they will be discussed in Sec. VI.

The phase diagram of $La_{1-x}Ca_xMnO_3$ for the low values of x, is similar to the phase diagram determined in $La_{1-x}Sr_xMnO_3$ by Kawano *et al.*[22] where, from $x \geqslant 0.075$, a ferromagnetic transition also appears at temperatures greater than T_N. In this x range, our phase diagram is different from that published by Schiffer *et al.*[23] We point out that we have not detected superstructure reflections compatible with a charge ordering for low doping, as reported in (Ref. 24). Instead, we have observed an elastic diffuse scattering showing a nearly isotropic q modulation characteristic of a magnetic short-range order.[21]

Finally, in the compound with $x=0.08$, as well as in the pure compound, well-defined antiferromagnetic (AF) spin correlations persist at temperatures much higher than T_N (Fig. 5). However, they are much less developed in the $x=0.05$ compound. This can be explained by the presence in this latter compound, of isolated, noninteracting magnetic impurities Mn^{4+}. Indeed, in that case, we have found localized magnetic impurity modes, observed by inelastic neutron scattering.[20] The reduction of AF correlations might be related to the value of the critical exponent β of the order parameter (Fig. 1). The value observed for $x=0.05$ (0.43) is rather close to that given by the mean-field Landau theory (0.5) where fluctuations are neglected. These isolated Mn^{4+} ions should prevent the growth of the AF correlation length, except in the close vicinity of T_N.

IV. SPIN WAVES

In the following we present inelastic neutron-scattering measurements for the $x=0.08$ compound and compare them with those obtained in pure and in $x=0.05$ doped compounds. In pure $LaMnO_3$ we have detected only one spin-wave branch. Its dispersion may be related to the superexchange coupling between Mn ions and the gap measured in this branch has been attributed to the single-ion anisotropy.[17] For the $x=0.05$ sample, in addition to the ''superexchange'' spin waves, new spin dynamics appear. These excitations are

TABLE I. Summary of values of the cant angle, magnetic transition temperatures, exchange integrals, anisotropy, gap and stiffness of the extra branch $\omega=\omega_0+Dq^2$ for the three studied samples.

x	θ (deg)	T_N (K)	T_C (K)	J_1 (meV)	J_2 (meV)	C (meV)	ω_0 (meV)	D (meV Å^2)
0		139.5 ± 0.3		0.83 ± 0.04	-0.58 ± 0.02	0.17 ± 0.008		
0.05	5 ± 1	133 ± 0.3	123 ± 0.3	0.91 ± 0.04	-0.33 ± 0.02	0.15 ± 0.008	0.91 ± 0.02	4.5 ± 0.1
0.08	13 ± 1.5	122 ± 0.3	126 ± 0.3	1 ± 0.04	-0.28 ± 0.02	0.16 ± 0.008	0.5 ± 0.02	7.3 ± 0.1

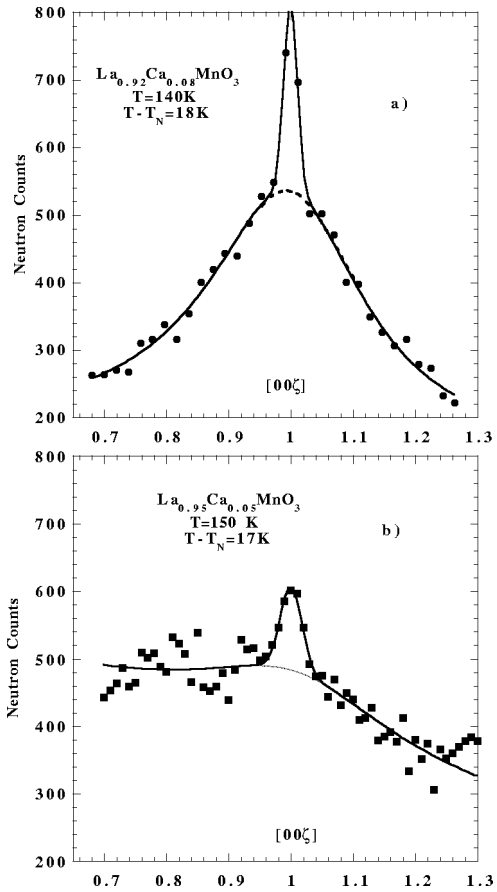

FIG. 5. Antiferromagnetic correlations. (a) $La_{0.92}Ca_{0.08}MnO_3$, $T=140$ K, $(T-T_N=18$ K), $k_i=1.55$ Å^{-1}. The correlation length is ≈ 8 Å. (b) $La_{0.95}Ca_{0.05}MnO_3$, $T=150$ K, $(T-T_N=17$ K), $k_i=2.662$ Å^{-1}, spectrum measured with a double-axis spectrometer; AF correlations are very small (see text). The small peaks riding the Lorentzian profiles are due to the second-order harmonic in the incident beam reflected by the (002) Bragg peak, revealed because of a long-counting time.

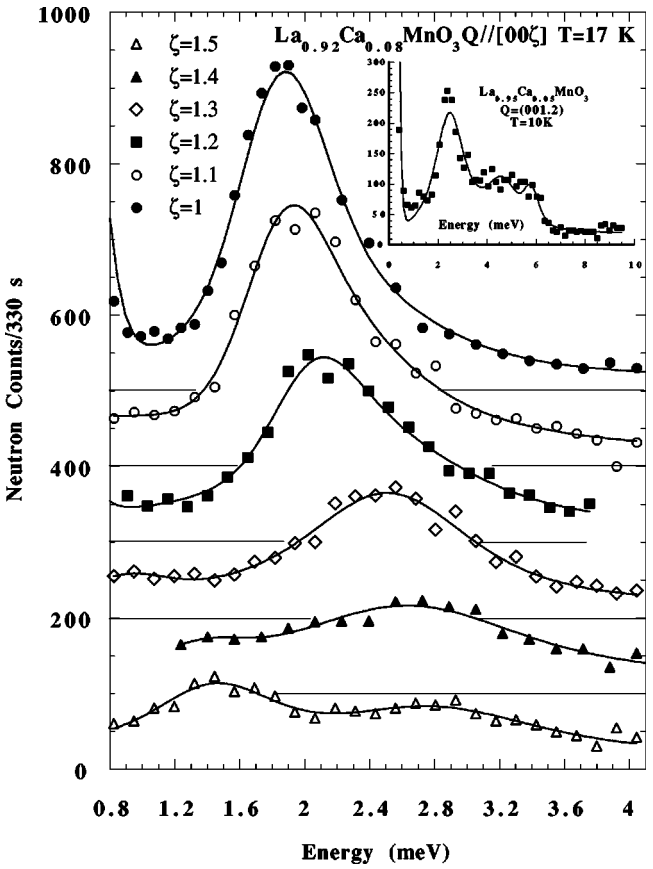

FIG. 6. Inelastic spectra taken at $\mathbf{q}=(00\zeta)$ at 17 K in $La_{0.92}Ca_{0.08}MnO_3$. For the sake of clarity, an offset of 100 is added to each spectrum. The dispersion of the spin waves is clearly seen from the center to the zone boundary where an additional peak appears at smaller energy. This is the zone boundary excitation belonging to the low-energy spin-wave branch measurable only in the (002) zone (see text). The inset shows a similar energy scan measured in $La_{0.95}Ca_{0.05}MnO_3$ at $\mathbf{Q}=(001.2)$. We can see that localized magnetic impurity modes appear from 3.5 to 6 meV. They do not exist in $La_{0.92}Ca_{0.08}MnO_3$. The lines are the best fits given by the convolution of $S(\mathbf{q},\omega)=[n(\hbar\omega)+1][\text{const}/[(\omega-\omega_{\mathbf{q}})^2+\Gamma_{\mathbf{q}}^2]$ with the spectrometer resolution function.

located in a lower-energy range and coexist with localized magnetic impurity modes.[20]

A. High-energy spin-wave branch

Similarly to the pure and the $x=0.05$ samples, in the $x=0.08$ compound we have focussed on the spin waves propagating along [001] starting from the AF peak (001) and along [110] starting either from the AF Bragg peak (111) where the dynamical structure factor (i.e., the root of the intensity of scattered neutrons) is maximum at low q values,[25] or from the F Bragg peak (110) in other cases. In Fig. 6 we present some experimental spectra registered along [001] at low temperature ($T=17$ K). From similar spectra, we have deduced the spin wave energies and their q dispersion. In spite of the disorder induced by doping, we may see that the damping of these modes is very small at $q=0$ and slightly increases until the zone boundary. At this point ($\zeta=1.5$), the spectrum exhibits a second peak at a lower energy that belongs to another spin-wave branch, as it will be discussed below. For $x=0.08$, the observations of propagative modes have been easier than for $x=0.05$ because they are not shaded by local modes[20] (see inset of Fig. 6). All measurements concerning the three samples in this range of energy are displayed in Fig. 7 with empty symbols.

In the three compounds, this ''high energy'' spin-wave branch exhibits a gap. Surprisingly, the value of the gap abruptly changes from 2.6 meV in the pure compound to 1.8 meV for both $x=0.05$ and $x=0.08$. The energies of spin waves are lower for $x=0.08$ than for $x=0.05$ along the direction [001]. In contrast, in the basal ferromagnetic plane, along the [110] direction, the energies slowly increase with Ca doping.

These spin-wave dispersion curves have been associated with a superexchange coupling renormalized by the double exchange, only first-neighbor interactions through oxygen bonds are considered. We describe the spin system by a Heisenberg Hamiltonian with single-ion anisotropy as in Ref. 17:

$$\mathcal{H}=-\sum_{i,j} J_{ij}\mathbf{S}_i\mathbf{S}_j-C\sum_i S_i^{z2}.$$

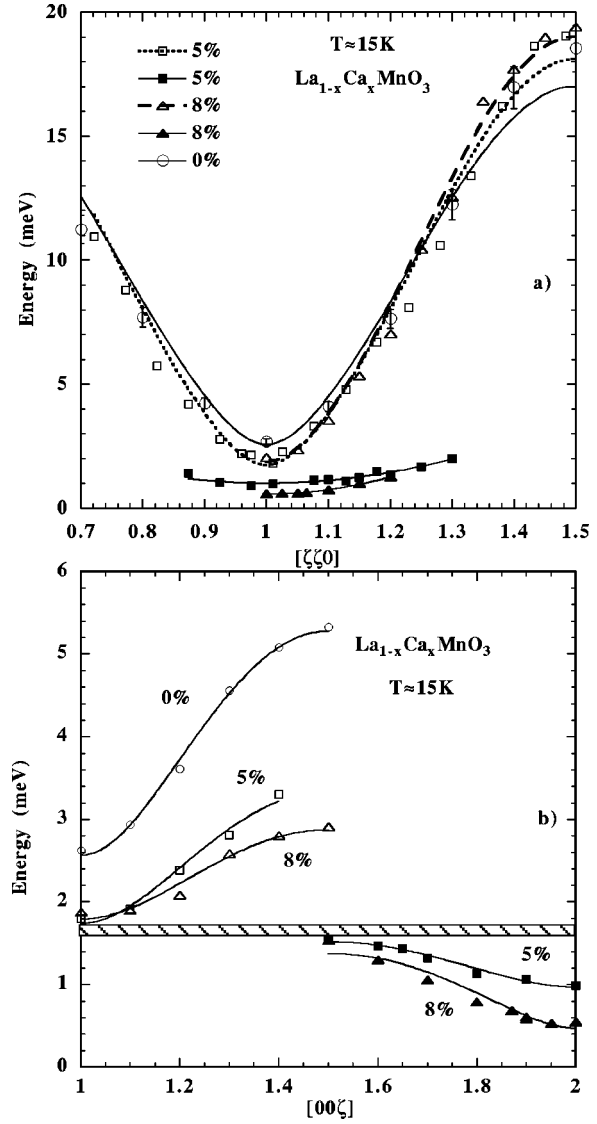

FIG. 7. Spin-wave dispersion curves for pure and doped compounds. (a) Along the [110] direction. (b) Along the [001] direction. Empty symbols represent spin waves related to superexchange. The lines through them are fitted dispersion laws resulting from the diagonalization of a Heisenberg Hamiltonian. Full symbols represent the new spin-wave branches connected to the magnetic coupling induced by doping (see text). In this latter case, lines are guides for the eye. Hatched area represents a narrow energy band separating both kinds of spin waves.

In this model, the anisotropy term is responsible for the gap observed in the spin-wave spectra. Two exchange integrals are needed: $J_1>0$, a ferromagnetic coupling between first neighbors in the basal plane (a,b) and $J_2<0$, an antiferromagnetic coupling between first neighbors along the c axis (Fig. 3). The classical Holstein-Primakoff approximation for spin waves propagating with the reduced wave vector $\mathbf{q}=q_H a^*+q_K b^*+q_L c^*$ is used. The following dispersion law is deduced:

$$\omega(\mathbf{q})=2S\sqrt{A(\mathbf{q})^2-B(\mathbf{q})^2},$$

$$A(\mathbf{q})=A(q_H,q_K,q_L),$$

$$A(q_H,q_K,q_L)=2J_1\{2-\cos[\pi(q_H+q_K)]-\cos[\pi(q_H-q_K)]\}-2J_2+C,$$

$$B(\mathbf{q})=B(q_H,q_K,q_L)=2J_2\cos(\pi q_L),$$

$$S=2.$$

The values of J_1, J_2, and C have been obtained as follows: J_2 and C have been determined from the fit of the dispersion curve along the [001] direction [Fig. 7(b)] with the expression of $\omega(0,0,q_L)$ deduced from the above relations. Then, these two values of J_2 and C have been kept constant during the fitting process of the dispersion curve along the [110] direction [Fig. 7(a)], which has provided the value of J_1.

It can be seen in Fig. 7 that this model agrees rather well with the experimental data except for a small discrepancy in the the [110] direction. As seen from Fig. 7(b) and Fig. 7(a), the antiferromagnetic coupling $|J_2|$ that is responsible for the dispersion of the spin waves along c^*, decreases as x increases, while the ferromagnetic coupling J_1 that is responsible for the dispersion of the spin waves in the basal plane, increases. This behavior is generally explained by the increasing influence of the double-exchange coupling upon doping. Indeed, the hopping of mobile charge and spin carriers is favored by ferromagnetism, therefore the increase of carrier density strengthens the ferromagnetism and lowers the antiferromagnetism. The numerical results are summarized in Table I. In the case of pure $LaMnO_3$ our results very nicely compare with the predictions given by Feinberg *et al.*[26] and by Olés.[27] These authors calculate J_1 and J_2 from a spin-orbital model which fulfills the symmetry conditions for $S=2$ spins and where the Jahn-Teller effect plays a predominant role. In a recent paper, Feiner and Olés[28] apply the same theory to the case of doped compounds where exchange integrals are ''renormalized'' by the Mn^{4+} ions. Our results are in a good qualitative agreement with these calculations.

B. Low-energy spin-wave branch

As already observed for $x=0.05$,[20] in addition to the ''superexchange'' spin-wave branch, for $x=0.08$ we have also observed a branch of well-defined and dispersed magnetic excitations. As an example, inelastic spectra registered along the [110] direction, starting from the (110) Bragg peak, are shown in Fig. 8. In Fig. 7, we have represented these new branches (full symbols) together with ''superexchange'' spin waves for both Ca-doped crystals. Interestingly the local magnetic modes existing in the 5% compound are no longer observed for $x=0.08$, this seems to indicate that the local modes are typical of the lowest doping range.[5] Furthermore, the inelastic neutron-scattering intensities are stronger for higher doping values. As x increases, the low-energy spin-wave branch becomes more and more prevailing at expense of the exchange spin-wave branch (in particular along [110]). Preliminary results on a $x=0.1$ Ca-doped compound confirm these observations. These extra magnetic excitations have been measured following three directions: along [001] starting from the (002) Bragg peak, along [110] starting from the (110) Bragg peak, and along [112] starting from the (112) Bragg peak. The measured energies as well as the energy-

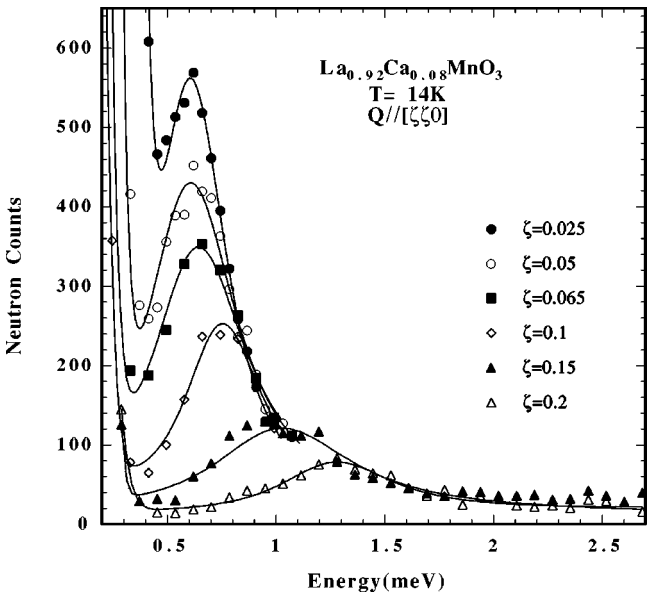

FIG. 8. Energy scans of the new spin-wave branch at different values of **q** along [110] at 14 K. Note the strong change in the intensity with increasing **q**.

integrated intensities are plotted versus q values in different directions in Fig. 9(a) and 9(b). These new spin waves have several specific features: (i) their energies are always within the gap of the ''superexchange'' spin waves. (ii) They have a ferromagnetic character, indeed they cannot be measured around any Bragg peak associated to antiferromagnetic order $(h,h,2l+1)$. However, they display the symmetry of the canted antiferromagnetic lattice since they flatten at (0,0,0.5), the zone boundary in [001] direction (the zone boundary cannot be reached along [110] because of vanishing intensity). So, they behave as *true magnetic eigenmodes* of the whole system. (iii) The intensity of these excitations in dependence on the direction of propagation, is described by the geometrical factor $1+\tilde{k}_z^2$ (with $\tilde{k}_z$ as the component of the unit vector $\mathbf{Q}/|Q|$ along the magnetization axis). This suggests that the spin components involved in this motion remain more or less confined in the *b*, *c* plane, but the twinning of the crystals does not allow us to be more conclusive. (iv) Assuming a dispersion law for low q values: $\omega=\omega_0+Dq^2$, the gap ω_0 of this extra spin wave branch strongly decreases with *x*, while the gap of the high-energy branch remains constant with *x*. The stiffness constant D appears nearly isotropic [see Fig. 9(a)], it increases upon doping. (v) Another very interesting result related to these extra spin-wave modes concerns their intensity. Inspection of spectra displayed in Fig. 8 evidences that the intensity of these modes steeply decreases with increasing q. Indeed, their energy-integrated intensity $S(\mathbf{q})=\int S(\mathbf{q},\omega)d\omega$ does not have the normal spin-wave behavior $\sim 1/\omega_q$, where ω_q is the spin-wave energy for the propagating vector **q**, predicted by Mori and Kawasaki on the basis of the Heisenberg model.[29] $S(\mathbf{q})$ appears to fall down rapidly up to $q\simeq 0.2$ Å^{-1} [see Fig. 9(b)]. This suggests the existence of instantaneous ferromagnetic correlations inside the mean canted AF structure. If $S(\mathbf{q})$ is fitted with a Lorentzian law, a characteristic correlation length of ≈ 9 Å is found. The last feature may be related to the results of recent elastic neutron-scattering

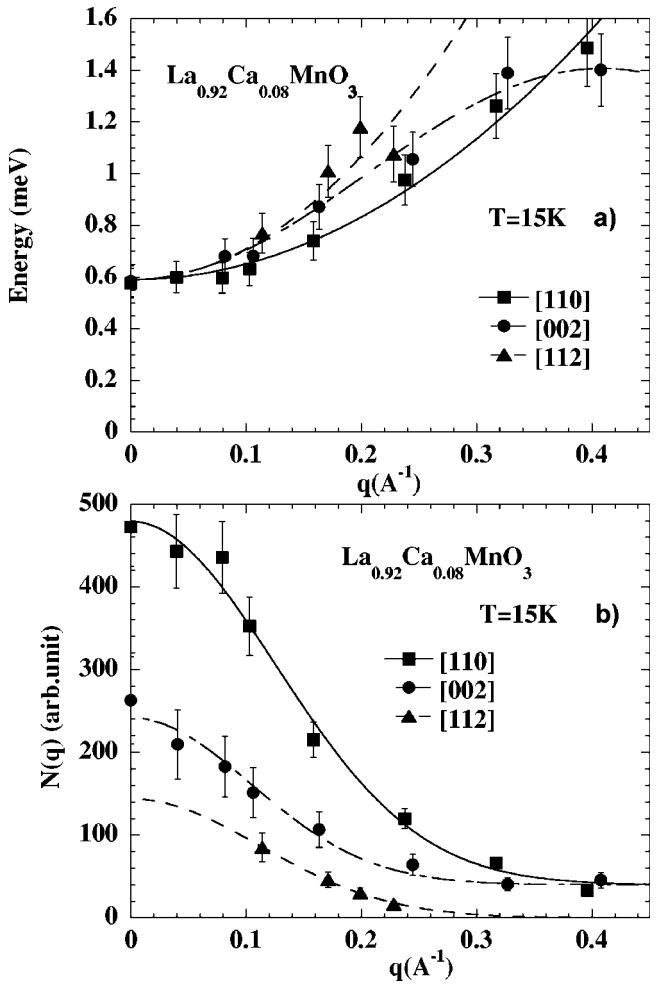

FIG. 9. (a) New spin-wave branches in different directions. (b) Energy-integrated intensity $N(\mathbf{q})$ of the new spin-wave branches.

measurements[21] that revealed the existence of static magnetic inhomogeneities or droplets. The clusters have an average size similar to the correlation length of the low-energy excitations. All these features of the low-energy spin waves were already present in the $x=0.05$ compound,[20] but in the case of $x=0.08$ they are more enhanced.

V. TEMPERATURE BEHAVIOR OF SPIN WAVES

Now we present the behavior of both types of spin waves as a function of the temperature. We shall concentrate on the 8% compound. The magnons at $\mathbf{q}=0$, $\mathbf{q}=(0.25,0.25,0)$ and (0.5,0.5,0) of the high-energy spin-wave branch have been selected. The variations of their energies with temperature are reported in Fig. 10. This ''superexchange'' spin-wave branch behaves as expected for usual localized spin lattices in insulators [see, for instance, the study of spin waves in EuO (Ref. 30)]. As the temperature is approaching T_N, long wavelength magnons smear out into the hydrodynamic regime ($\mathbf{q}\rightarrow 0$, $\omega\rightarrow 0$) while the energy of short wavelength magnons, although renormalized, remains finite, even above T_N. Note the two different scales of energy in Fig. 10, the one for the gap and the other one for the two large q-value magnons.

The temperature behavior of the low-energy spin-wave

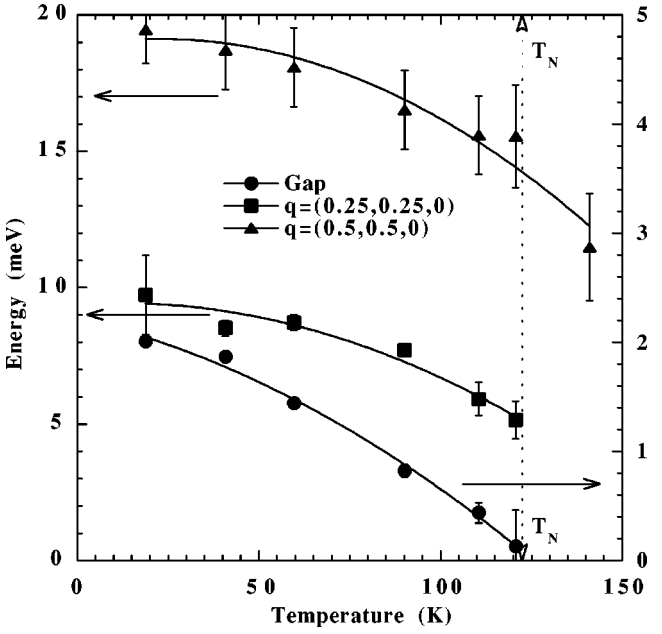

FIG. 10. Renormalization of superexchange magnons upon temperature increase. Note the change of energy scale for the gap on the right side of the figure.

branch has also been investigated. As an exemple, spectra taken at $\mathbf{Q}=(0,0,2.1)$ at different temperatures below T_N are displayed in Fig. 11. They show a strong energy renormalization as T approaches T_N. The corresponding values, deduced from a fit to a Lorentzian law, are depicted in the inset of Fig. 11. Then, around T_N, the scattering becomes quasielastic, which is characteristic of a diffusive mode. The spectra measured at T_N and at T_N+18 K are shown in Fig. 12. It is clearly seen that a well-formed quasielastic peak stands out from the elastic incoherent scattering. Within this low energy range, the damped ''superexchange'' spin waves ap-

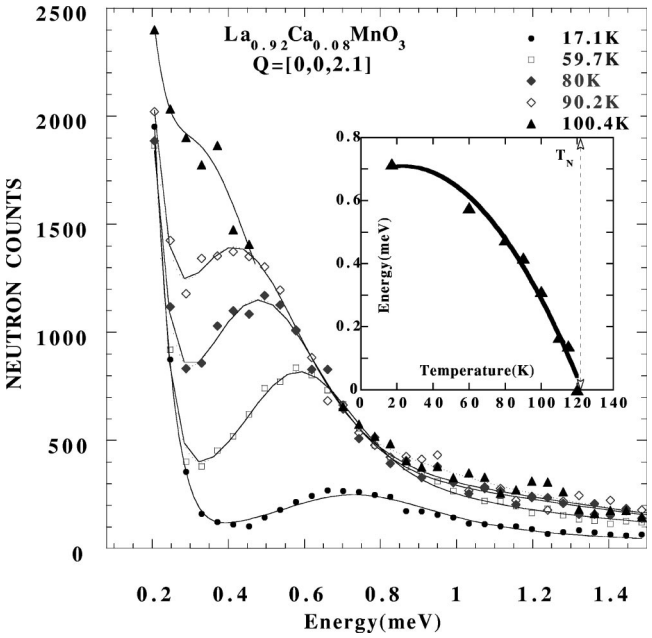

FIG. 11. Spectrum of a magnon of the new spin-wave branch, at $\mathbf{q}=(0,0,0.1)$, at various temperatures. In the inset, the temperature behavior of its energy $\omega_{\mathbf{q}}$ is represented.

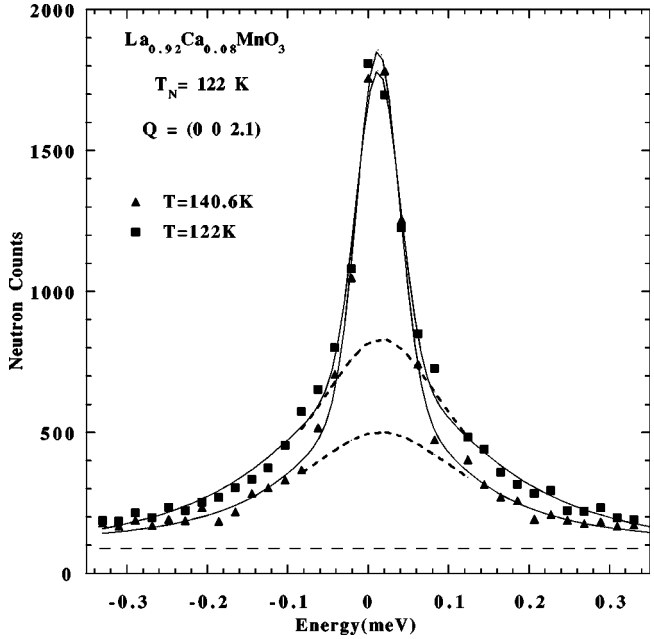

FIG. 12. Quasielastic spectra measured at $Q=(002.1)$ at 122 K and 140.6 K. Dotted lines represent fits with a Lorentzian law. In this energy range, the quasielastic scattering by damped superexchange spin waves spreads along like a constant background.

pear as a flat background. In Fig. 13 we have represented the energy-integrated intensity $N(\mathbf{q})$ of this peculiar mode at $\mathbf{Q}=(0,0,2.1)$, $(\mathbf{q}=0.1)$, in the whole studied temperature range, in the ordered magnetic phase as well as above T_N. $N(\mathbf{q})$ is defined from the scattering function $S(\mathbf{q},\omega)$, that is proportional to the product of the Bose factor by a generalized susceptibility: $[1+n(\hbar\omega)]\chi(\mathbf{q},\omega)$, so $N(\mathbf{q})=\int\chi(\mathbf{q},\omega)d\omega$ behaves as a magnetic susceptibility $\chi(\mathbf{q})$. It increases with temperature, exhibits a maximum around T_N, and then decreases above T_N.

Furthermore, at T_N we have measured the quasielastic scattering *all along* the [001] direction, starting from the

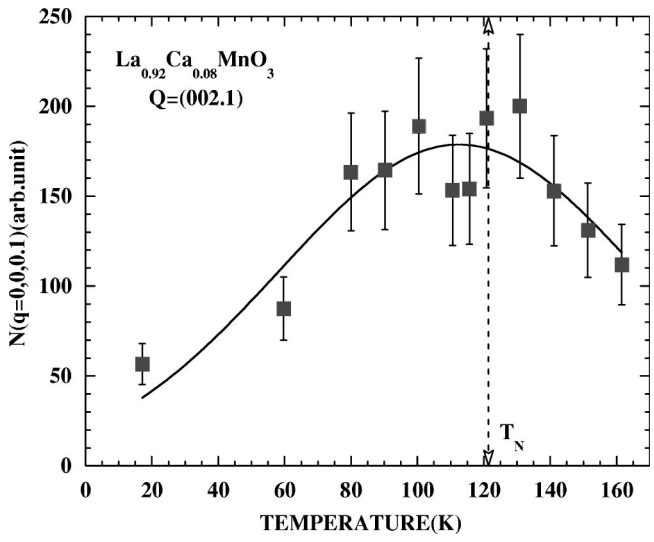

FIG. 13. Energy-integrated intensity $N(\mathbf{q})$ at $\mathbf{q}=(0,0,0.1)$ versus temperature. (The effect of Bose factor has been taken into account.) Note the maximum around the Néel temperature ($T_N=122$ K).

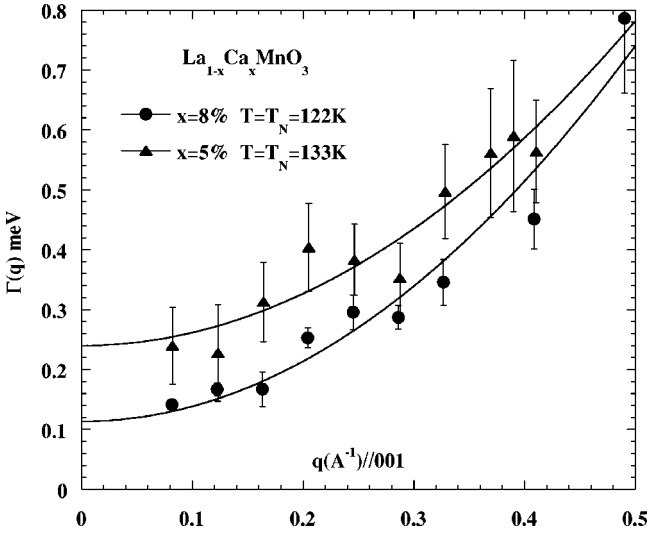

FIG. 14. Comparison of the dispersion of the energy width of quasielastic scattering at T_N for both 5% and 8% compounds.

point (002.1). In contrast to the ''superexchange'' branch where only long wavelength magnons become diffusive modes at T_N, *all spin waves* related to this new branch renormalize to zero energy and lose their character of collective mode. The quasielastic scattering function can be fitted by a lorentzian law, centered on zero energy and with a width $\Gamma(q)$: $S(\mathbf{q},\omega) \propto 1/[\omega^2+\Gamma(q)^2]$. We have found that the dispersion of the width $\Gamma(q)$ follows approximately a law of the form: $\Gamma(q)=\Gamma_0+dq^2$. Similar measurements have been performed on the $x=5\%$ compound ($T_N=133$ K). The behavior of $\Gamma(q)$ for both compounds is shown in Fig. 14. We observe that d increases with x while Γ_0 decreases. The dispersion law of the width $\Gamma(q)$, as well as the variation of Γ_0 and d with x, is similar to the behavior of the dispersion law of the low-energy spin wave $\omega=\omega_0+Dq^2$ at low temperature (see Table I). Moreover, the finite value of Γ_0 prevents the divergence of $\chi(\mathbf{q})$ at T_N.

Finally, Fig. 15 presents, in comparable units, the energy-integrated scattering intensity $N(\mathbf{q})$, measured at T_N for both compounds. Two important aspects deserve to be mentioned:

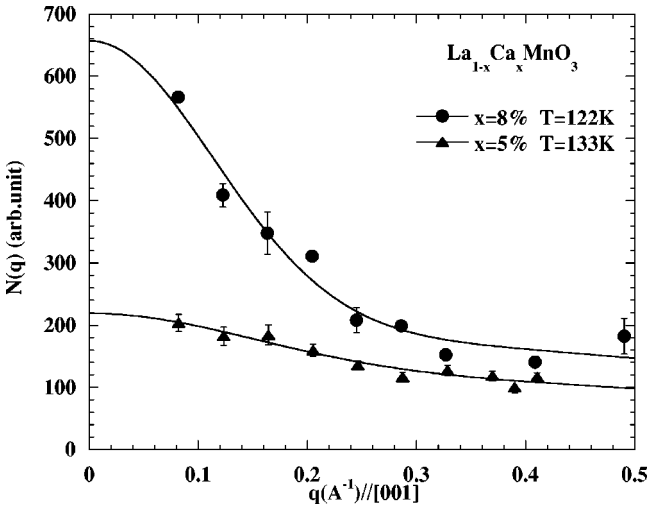

FIG. 15. Comparison of the energy-integrated intensity $N(\mathbf{q})$ of quasielastic scattering at T_N for both 5% and 8% compounds.

(i) $N(\mathbf{q})$ is higher in the case of larger x. The two $N(\mathbf{q})$ values differ by a factor of at least 2. This supports the idea that the new spin excitations are related to the charge carriers introduced by doping. (ii) The q dependence of $N(\mathbf{q})$ reflects the existence of instantaneous ferromagnetic correlations. These correlation lengths, as measured at T_N, appear smaller than those measured at low temperature and they weakly depend upon x. So, the temperature behavior of the excitations confirms the magnetic character of the new branch and its specific features that are different from these of the spin waves related to superexchange.

VI. DISCUSSION AND CONCLUSION

Our measurements demonstrate that, in the low doping regime, two kinds of magnetic coupling exist in the Ca-doped perovskites as revealed by two branches of spin waves. One is easily attributed to superexchange coupling, renormalized by the doping. The ferromagnetic exchange in the basal planes increases with x, while antiferromagnetic exchange along c decreases with x. The lifting of degeneracy of the spin waves in the canted AF system cannot be put forward to explain all the features of the low-energy spin-wave branch. In particular, the canting angle is too small to explain the observed values of energy gaps. These extra magnetic excitations have specific features distinct from superexchange spin waves in insulators: (i) they appear with doping and are of ferromagnetic character since they can be measured only around F Bragg peaks. (ii) Their dynamical magnetic structure factor indicates some kind of short-range ferromagnetic order. (iii) When compared to high-energy excitations, they exhibit a different temperature behavior. Moreover, from these results, and our recent elastic diffuse scattering measurements,[21] a weakly inhomogeneous magnetic phase emerges leading to a scheme of hole-poor and hole-rich regions (Mn^{4+} or O^- ions). This resembles the theoretical predictions of electronic phase separation,[5–8] although not achieved in the present case. As mentioned in Sec. III, some arguments are in favor of a canted antiferromagnetic state and not in favor of a coexistence of F and AF regions. (i) If F regions should exist, we should have measured nearly isotropic spin waves, which is not the case ($J_1>0$, $J_2<0$). As to the new spin wave branch related to the doping, although isotropic at low q values and of ferromagnetic nature, it is symmetric with respect to the zone boundary in the c^* direction, which is characteristic of the AF order. (ii) Moreover, recent measurements on Bragg peaks under applied magnetic field strengthen this picture. This will be published elsewhere.[31]

A first attempt to explain the dispersion law of the low-energy magnetic excitations could be to use the double-exchange model. This model couples the probability of hopping of the charge carriers to the ferromagnetism. The stiffness constant D is predicted to be connected to the double-exchange coupling responsible of the canted AF ground state [$D \propto \sin(\theta)$] by de Gennes.[15] As the canting angle θ is small, it would induce a small value of D. But this mean-field model does not explain all of our results, in particular the inhomogeneous features. We could also assume that holes are mobile inside the droplets making them quasimetallic. Then, the stiffness constant D of the new spin-wave

branch could be related to the width of the conduction band and to x as proposed by the model for ferromagnetic metals of Kubo and Ohata.[32] In this framework the quasimetallic inhomogeneities could be the precursor effects announcing the ferromagnetic metallic phase observed above the critical value of doping: $x_c \simeq 16\%$. D could be small because of the small values of x and the weak conduction bandwidth. Actually, the strong distortion of the oxygen octahedra modifies the hybridization between d orbitals of Mn and p orbitals of O and induces a narrow electronic conduction band. Another explanation could be that D is connected with the weak coupling between the droplets through the average magnetic lattice. This coupling would be possibly responsible of their liquidlike organization.[21] Moreover the gap of the new branch could be due to an anisotropy of the net magnetization of these droplets that might be smaller than the anisotropy of the mean magnetic lattice. Other possible couplings responsible for these new spin dynamics can also be mentioned, as, for example, the coupling of the spins with the long-range ordered Jahn-Teller distortion as introduced by Millis[2] and Rőder *et al.*[33] To detect any lattice or atomic mode component requires polarized neutron experiments that have not yet been performed to our knowledge. Until now all our measurements, and especially the temperature-dependent studies, have shown that the magnetic character is dominant.

There are very few spin excitation studies on doped manganites in the low doping regime. In the case of La compounds weakly doped with Sr, to our knowledge, published neutron-scattering measurements do not mention any further low-energy spin waves.[19,39] However, recent antiferromagnetic resonance measurements on Sr-doped compounds reveal two distinct modes for $x = 0.05$ that might be related to our observations.[40] In contrast, many neutron-scattering works exist on highly doped systems that display a metal-insulator transition. Clausen *et al.*[34] use the concept of magnetic polarons[35] to interpret their diffuse coherent quasielastic neutron-scattering experiments. Lynn *et al.*[36] find ''unusual'' relaxational spin correlations in addition to normal spin waves, in a polycrystalline Ca-doped compound with $x = 33\%$. De Teresa *et al.*[37] associate the ''small polaron'' concept to ferromagnetic clusters in order to explain the anomalies appearing at T_C in polycrystalline $x = 33\%$ Ca-doped compound. Fernandez-Baca *et al.*[38] also invoke magnetic clusters at T_C in a similar case. All these findings are related to the present results, except that, *at low values of doping rate*, these ferromagnetic inhomogeneities can develop within a canted antiferromagnetic phase so that their specific magnetic coupling can be revealed by propagation of collective excitations. How do the spin dynamics evolve from the double-branch state reported here into a state with only one branch characteristic of a ferromagnetic metallic phase? Future work on $x = 0.1$ and $x = 0.15$ Ca doped compounds should answer this question.

ACKNOWLEDGMENTS

It is a pleasure to thank Dr. A. M. Oleś for stimulating discussions and M. Braden for discussions and critical reading of the manuscript.

[1] C. Zener, Phys. Rev. **82**, 403 (1951).
[2] A. J. Millis, P. B. Littlewood, and B. I. Shraiman, Phys. Rev. Lett. **74**, 5144 (1995).
[3] C. M. Varma, Phys. Rev. B **54**, 7328 (1996).
[4] D. I. Khomskii and G. A. Sawatzky Solid State Commun. **102**, 87 (1997).
[5] M. Kagan, D. Khomskii, and M. Mostovoy, cond-mat/9804213 (unpublished).
[6] E. L. Nagaev, Phys. Status Solidi B **186**, 9 (1994).
[7] J. Riera, K. Hallberg, and E. Dagotto, Phys. Rev. Lett. **79**, 713 (1997).
[8] S. Yunoki, J. Hu, A. L. Malvezzi, A. Moreo, N. Furakawa, and E. Dagotto, Phys. Rev. Lett. **80**, 845 (1998).
[9] J.-S. Zhou and J. B. Goodenough, Phys. Rev. Lett. **80**, 2665 (1998).
[10] I. F. Lyuksyutov and V. Prokrovsky, cond-mat/9808248 (unpublished).
[11] S. Jin, T. H. Tiefel, M. McCormack, R. A. Fastnachrt, R. Ramesh, and L. H. Chen, Science **264**, 413 (1994).
[12] J. L. Fontcuberta, B. Martínez, A. Seffar, S. Piñol, J. L. García-Muñoz, and X. Obradors, Phys. Rev. Lett. **76**, 1122 (1996).
[13] J. B. Goodenough, Phys. Rev. **100**, 564 (1955).
[14] E. O. Wollan and W. C. Koehler, Phys. Rev. **100**, 545 (1955).
[15] P. G. de Gennes, Phys. Rev. **118**, 141 (1960).
[16] G. Matsumoto, J. Phys. Soc. Jpn. **29**, 3336 (1970).
[17] F. Moussa, M. Hennion, J. Rodríguez-Carvajal, H. Moudden, L. Pinsard, and A. Revcolevschi, Phys. Rev. B **54**, 15 149 (1996).
[18] J. Rodríguez-Carvajal, M. Hennion, F. Moussa, H. Moudden, L. Pinsard, and A. Revcolevschi, Phys. Rev. B **57**, R3189 (1998).
[19] K. Hirota, N. Kaneko, A. Nishizawa, Y. Endoh, M.C. Martin, and G. Shirane, Physica B **237-238**, 36 (1997).
[20] M. Hennion, F. Moussa, J. Rodríguez-Carvajal, L. Pinsard, and A. Revcolevschi, Phys. Rev. B **56**, R497 (1997).
[21] M. Hennion, F. Moussa, J. Rodríguez-Carvajal, L. Pinsard, and A. Revcolevschi, Phys. Rev. Lett. **81**, 1957 (1998).
[22] H. Kawano, R. Kajimoto, M. Kubota, and H. Yoshizawa, Phys. Rev. B **53**, R14 709 (1996).
[23] P. Schiffer, A. P. Ramirez, W. Bao, and S-W. Cheong, Phys. Rev. Lett. **75**, 3336 (1995).
[24] A. J. Millis, Nature (London) **392**, 147 (1998).
[25] S. W. Lovesey, *Theory of Neutron Scattering from Condensed Matter* (Clarendon Press, Oxford, 1987), Vol. 2, p. 118.
[26] D. Feinberg, P. Germain, M. Grilli, and G. Seibold, Phys. Rev. B **57**, R5583 (1998).
[27] A. M. Oleś, J. Supercond. (to be published); L. F. Feiner and A. M. Oleś, Phys. Rev. B **59**, 3295 (1999).
[28] L. F. Feiner and A. M. Oleś, Physica B **259-261**, 796 (1999).
[29] H. Mori and K. Kawasaki, Prog. Theor. Phys. **27**, 529 (1962).
[30] H. A. Mook, Phys. Rev. Lett. **46**, 508 (1981).
[31] G. Biotteau, M. Hennion, F. Moussa, J. Rodríguez-Carvajal, L. Pinsard, and A. Revcolevschi (unpublished).
[32] K. Kubo and N. Ohata, J. Phys. Soc. Jpn. **33**, 21 (1972).
[33] H. Rőder, J. Zang, and A. R. Bishop, Phys. Rev. Lett. **76**, 1356 (1996).

[34] K. N. Clausen, W. Hayes, D. A. Keen, R. M. Kusters, R. L. McGreevy, and J. Singleton, J. Phys.: Condens. Matter **1**, 2721 (1989).
[35] T. Kasuya and A. Yanase, Rev. Mod. Phys. **40**, 684 (1968).
[36] J. W. Lynn, R. W. Erwin, J. A. Borchers, Q. Huang, and A. Santoro, Phys. Rev. Lett. **76**, 4046 (1996).
[37] J. M. De Teresa, M. R. Ibarra, P. A. Algarabel, C. Ritter, C. Marquina, J. Blasco, J. García, A. del Moral, and Z. Arnold, Nature (London) **386**, 256 (1997).
[38] J. A. Fernandez-Baca, P. Dai, H. Y. Hwang, C. Kloc, and S-W. Cheong, Phys. Rev. Lett. **80**, 4012 (1998).
[39] A. H. Moudden, L. Vasiliu-Doloc, L. Pinsard, and A. Revcolevschi, Physica B **241-243**, 276 (1998).
[40] V. Yu. Ivanov, V. D. Travkin, S. P. Lebedev, A. A. Volkov, A. Pimenov, A. Loidl, A. M. Balbashov, and A. V. Mozhaev, J. Appl. Phys. **83**, 7180 (1998).